Reliability Challenges in Fabrication of Flexible Hybrid Electronics for Human Performance Monitors: A System Level Study

Varun Soman, *Student Member, IEEE,* Yasser Khan, Madina Zabran, Mark Schadt, *Member, IEEE,* Paul Hart, *Member, IEEE,* Michael Shay, *Member, IEEE,* Frank Egitto, *Member, IEEE,* Konstantinos Papathomas, *Member, IEEE,* Natasha A. D. Yamamoto, Donggeon Han, Ana C. Arias, Kanad Ghose, *Member, IEEE,* Mark D. Poliks, *Member, IEEE* and James N. Turner

Abstract— **Flexible hybrid electronics (FHE) interface rigid electronic components with flexible sensors, circuits, and substrates. This paper reports the reliability improvement of a FHE Human Performance Monitor (HPM), designed to monitor electrocardiography (ECG) signals. The 50.8 mm × 50.8 mm HPM is fabricated on Kapton® HN polyimide (PI) substrate with flexible gold (Au) ECG electrodes on one side of the substrate and rigid electronic components for signal processing and communication mounted on the other side of the substrate. Our previously reported HPMs demonstrated reliability issues due to (1) cracking of the copper (Cu) circuitry, and (2) thinning and lack of adhesion at the printed Au and plated Cu interface that connected printed sensors to the Cu circuitry. Both failure mechanisms resulted in electrical opens in the circuit, which caused device failure. We explored effect of different design parameters, such as PI substrate thickness (50 µm vs 125 µm), Cu circuit thickness (2 µm vs 6 µm), solder reflow temperature (205 ˚C for Tin-Lead (Sn-Pb) vs 175 ˚C for Tin-Bismuth (Sn-Bi) solder), solder pad design, and optimized inkjet printing (printing on bare Cu vs Au plated Cu) on improving FHE reliability. Test vehicles (TVs) with different combinations of these factors were fabricated and bend tested to determine the most robust configuration. TVs with 50 µm thick PI substrate, 6 µm thick Cu circuit, Sn-Bi solder, redesigned solder pads with rounded corners, and printed Au traces on Au plated Cu pads demonstrated the best reliability results.**

***Index Terms*— Flexible electronics, Printed electronics, Flexible hybrid electronics, Robustness, Materials reliability, Bend testing, Wearable sensors**

I. INTRODUCTION

APPLICATIONS of wearable flexible hybrid electronics (FHE) that combine conformity and light weight of flexible circuitized sensor and substrates with the performance of traditional rigid electronic components are growing rapidly. Wearable sensors for human biometric performance monitoring, such as the Fitbit, Garmin Vivosmart and Apple Watch have recently seen a large increase in popularity. However, the desire for more technologically advanced wearable sensors is of increasing interest, especially in healthcare, wellness, and fitness areas. Flexible sensors that conform to the skin of human subjects are used to monitor motion [1], radial artery pulse waves [2], biomarkers in sweat [3-4], electrocardiography (ECG) signals [5], etc. Due to the conformal nature of these sensors, they can adhere to the skin and maintain a high-fidelity sensor-skin interface. This conformal contact with the skin allows them to record biosignals with a high signal-to-noise ratio [6-7].

For many of these flexible sensors designed to monitor biosignals, a limitation is that they often lack the required electronics for signal conditioning and communication, and therefore must be hard-wired to external electronics for these purposes [8-11]. Wireless solutions that feature electronics for signal conditioning and communication are either bulky or are not truly flexible [12-15]. To overcome these limitations, we previously proposed a solution where we combined flexible sensors with conventional rigid electronics, which had high computational efficiency with low power requirements, on a circuitized flexible substrate [16-19]. However, this introduced new reliability challenges since substrate flexibility may induce stresses in the electrical circuit that were not previously seen in comparable rigid circuit boards. A focused effort is needed to

This work was primarily funded by contract #FA86501327311-7 from the NanoBio Manufacturing Consortium through a program sponsored by the Air Force Research Laboratory. This material is also based, in part, on research sponsored by Air Force Research Laboratory under agreement number FA8650-15-2-5401 via FlexTech Alliance, Inc., as conducted through its flexible hybrid electronics manufacturing innovation institute. The U.S. Government is authorized to reproduce and distribute reprints for Governmental purposes notwithstanding any copyright notation thereon.

Varun Soman and Mark D. Poliks are with the Department of Systems Science and Industrial Engineering, Binghamton University, Binghamton, New York, 13902, USA and work in the Small Scale Systems Integration and Packaging (S3IP) Center.

Madina Zabran and Kanad Ghose are with the Department of Computer Engineering, Binghamton University, Binghamton, New York, 13902, USA and work in the Small Scale Systems Integration and Packaging (S3IP) Center.

James N. Turner is with the Small Scale Systems Integration and Packaging (S3IP) Center at Binghamton University, Binghamton, New York, 13902, USA.

Yasser Khan, Natasha A. D. Yamamoto, Donggeon Han, and Ana C. Arias are with the Department of Electrical Engineering and Computer Sciences, University of California, Berkeley, California, 94720, USA.

Mark Schadt, Paul Hart, Michael Shay, Frank Egitto, and Konstantinos Papathomas are with i3 Electronics, Endicott, New York, 13760, USA

This article has been accepted for publication in a future issue of this journal, but has not been fully edited. Content may change prior to final publication. Citation information: DOI 10.1109/TCPMT.2019.2919866, IEEE Transactions on Components, Packaging and Manufacturing Technology

understand and mitigate the factors affecting FHE device reliability, especially under their expected operating conditions. This is especially true since unlike the reliability of printed wiring boards, which is comparatively well-characterized and understood, FHE devices differ greatly in their susceptibility to the effects of thermal and mechanical stresses. Mechanical stresses (static or dynamic) introduced by one-time bends or repeated flexing of FHE devices will induce much higher strains as compared to rigid printed wiring boards.

Previous efforts have focused on studying the electrical and mechanical reliability of conductive traces fabricated on thin flexible substrates using a variety of techniques. These include electroplating, gravure printing, aerosol jet printing, inkjet printing, and screen printing [20-24]. Due to the flexibility of both the substrate and trace materials, flexible electronics need to be tested for failure under multiple failure modes that they are expected to be exposed to during real life use. Hence multiple studies have focused on failure modes such as bending, stretching and torsion [25]. Due to the physical nature of thin traces on flexible plastic films, the response of these materials to external loads is highly nonlinear. Therefore, experimental tests to characterize their behavior under such loads may not be easy to design. Hence studies have been done to create numerical models for such tests and correlate modeling results to experimental results [26-27]. However, the findings of these studies may not necessarily apply to conductive traces in a fully fabricated FHE device, as specimens tested in those studies do not take into account thermal stresses induced as a result of solder reflow processes for mounting conventional rigid electronics. Furthermore, it has been shown that the placement of rigid conventional silicon-based components affects flexibility as well as mechanical and electrical reliability [28]. Hence, it is important to perform reliability testing on fully fabricated FHE devices to understand the defects and failures that can be induced as a result of thermal stresses during solder reflow process and mechanical stresses during testing under the expected operating conditions of the FHE devices, as well as general handling. Given the problems found and the possible causes identified in our previous work [16-19], this report gives the detailed study undertaken to not only better understand the factors affecting plated and printed circuit line in these FHE devices, but also describes the changes implemented which were found to improve the reliability of the copper (Cu) circuits, printed gold (Au) traces and electrodes, and their interfaces.

II. Circuitization And Metal Interfaces

We previously reported the design and fabrication of Generation 1 (Gen. 1) human performance monitor (HPM) devices that monitored ECG signals using flexible printed Au electrodes and the associated reliability issues [16-19]. The Gen. 1 HPM device was fabricated on a 50.8 mm × 50.8 mm piece of 50 µm thick Kapton® HN polyimide (PI) substrate. Flexible Au ECG electrodes were printed on one side of the PI substrate (sensor side) whereas rigid electronic components for signal conditioning and communication were surface mounted on the other side using traditional solder reflow (component side) (Figure 1). The sensor side was electrically connected to the component side using plated through hole vias. The flexible printed sensors, circuits and the electronic components were

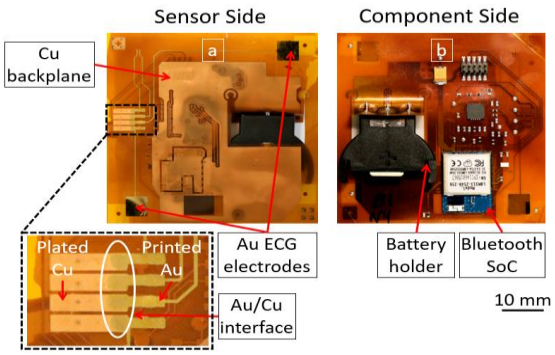

Figure 1. Sensor side (a) and component side (b) of the Gen. 1 HPM.

designed and dimensioned taking into account the overall device dimension constraints of 50.8 mm × 50.8 mm as well as our standard manufacturing processes and capabilities. The Gen. 1 HPM device fabrication process is described briefly here. 50 µm thick Kapton® HN polyimide (PI) films were first metalized using a DC-Magnetron sputtering system by depositing 5 nm metallic chrome (Cr) adhesion layer and 250 nm Cu in ultra-high purity argon environment. This thin Cr/Cu seed metal layer then served as a conductive metal base for pattern electroplating Cu circuits to a 2 µm thickness in a semi-additive plating and lithographic process. Cu electroplating was done in a copper sulphate/sulphuric acid bath with a bath temperature of 80 °C. Circuits were protected, and solder pad openings were defined on the component side using a photoimageable solder mask. For inkjet printing on the sensor side with Au nanoparticle ink, the surface energy of the PI was adjusted using tetrafluoromethane (CF_4) and oxygen (O_2) plasmas. Following the surface energy optimization step, Au traces (200 µm wide, 600 nm thick) and electrodes were inkjet printed on the sensor side. Next, solder mask protection was deposited on the sensor side, with patterned openings for the electrodes. Rigid electronic components were mounted using a traditional surface-mount technology solder reflow process using Tin-Lead (Sn-Pb) paste.

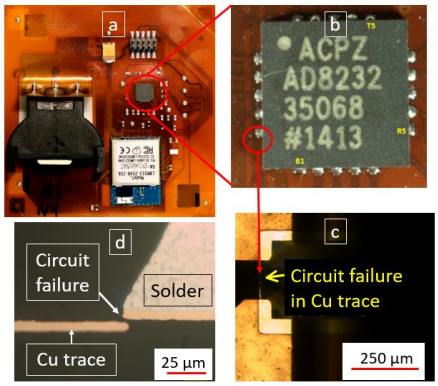

Figure 2. Component side of Gen. 1 HPM (a). Close-up of analog front-end chip (AD8232) showing all 20 solder joints (b). Crack in Cu trace (c). Cross-section showing failure in Cu trace (d).

It was noticed that the flexible Cu traces close to the analog front-end AD8232 signal conditioning chip in the Gen. 1 HPM were susceptible to cracking, causing an electrical open leading to device failure (Figure 2) [16][17]. The reasons might have been failure due to residual thermal stresses induced during the solder reflow process at die-attach, strains due to bending

This article has been accepted for publication in a future issue of this journal, but has not been fully edited. Content may change prior to final publication. Citation information: DOI 10.1109/TCPMT.2019.2919866, IEEE Transactions on Components, Packaging and Manufacturing Technology

caused by handling, or both. The solder was a Sn-Pb paste with a reflow temperature of 205 ˚C. The failure was consistently seen at the edge of the solder ball where the sudden change in stiffness creates a hinge point where stress is concentrated during bending (Figure 2).

The second source of electrical opens was found to be where printed Au traces overlapped onto Cu pads (Figure 1). These connections were used to interface the ECG electrodes with the rigid electronics. The printed Au to plated Cu interface demonstrated reliability issues in terms of thinning of printed Au and delamination from the Cu surface during thermal cycling. Contributing factors were identified as the surface energy mismatch of plated Cu and Kapton® HN PI to the printed ink traces. This resulted in non-uniform ink wetting on the Cu and the tendency of the ink to wick from the Kapton® HN substrate surface up onto the Cu interface pad resulting in thinning of the printed Au circuit line adjacent to the pad. The printed Au delamination from the contact pad was partly due to the formation of Cu oxide on the Cu pad prior to printing, reducing the reliability of the Au ink's adhesion to the Cu surface.

A. Cu circuitization failure modes and improvements

It was determined that Cu circuitry thickness, PI substrate thickness, the solder reflow temperature and the solder pad design might be the factors affecting the reliability of the Cu circuitry. Two sets of Test Vehicles (TVs) with fully assembled HPM component sides were fabricated and tested to study the effects of change in these variables on device reliability. In the first set, the TVs were fabricated using different combinations of substrate and Cu trace thicknesses, and either Sn-Pb or Tin-Bismuth (Sn-Bi) solder (reflow temperatures: 205 ˚C and 175 ˚C, respectively) (Figure 3). The lower reflow temperature of Sn-Bi solder was predicted to reduce the thermal stresses resulting from the coefficient of thermal expansion mismatch. These TVs were fabricated to study the effect of the parameters listed above on Cu circuit reliability only. Hence, these TVs did not have Au electrodes. For this reason, the surface energy optimization step described in the process for fabrication of Gen. 1 HPM devices was not carried out. The Gen. 1 HPM also had a Cu ground plane on the sensor side (Figure 1) that was eliminated on the TV's so that any circuit defects could be detected by inspection under an optical microscope. This was also done to test the Cu circuit reliability independent of the ground plane as future designs could have very different ground plane design or no ground plane at all. Table 1 shows the configurations of the first set of TVs fabricated in this study.

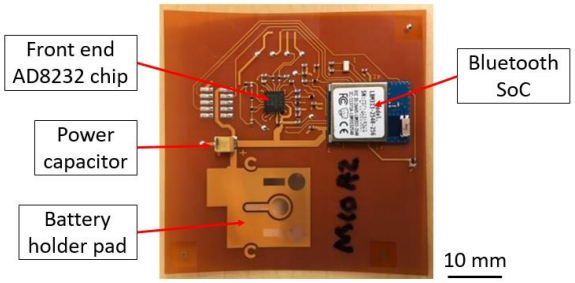

Figure 3. Component side of the HPM TV for evaluating Cu trace failures.

The second set of TVs was similar to the first set, but was fabricated using a new solder pad design aimed at reducing stresses at solder joint locations. The devices were fabricated using 50 µm thick Kapton® HN PI substrates, 2 µm thick Cu traces, and either Sn-Pb or Sn-Bi solder. The aim was to determine if the new solder pad design and the lower reflow temperature solder resulted in improved reliability. The new solder pad design utilized wider traces and rounded corners to reduce stresses at the solder pad/trace connection. The solder mask also fully captured both ends of the solder pads, including where the circuit transitions and connects to the pad. In the original solder pad design, the location where the circuit connects to the solder pad was not covered by the solder mask. The edge of the solder ball also sat at the same location as shown in Figure 4. In the modified solder pad design, the transition point of the circuit to solder pad was covered with solder mask. The edge of the solder ball was also pushed away from this point. This helped to reduce stress and increase stiffness at the transition point.

TABLE 1
GEN 1. AND SET 1 TV CONFIGURATION. NOTE: BOTH SOLDERS ARE THEIR EUTECTIC COMPOSITIONS

TV No.	Cu trace thickness (µm)	PI substrate thickness (µm)	Solder used
Gen. 1	2	50	Sn-Pb
1	6	50	Sn-Pb
2	6	50	Sn-Pb
3	6	50	Sn-Pb
4	6	50	Sn-Pb
5	6	50	Sn-Bi
6	6	50	Sn-Bi
7	2	125	Sn-Pb
8	2	125	Sn-Pb
9	2	125	Sn-Bi
10	2	125	Sn-Bi

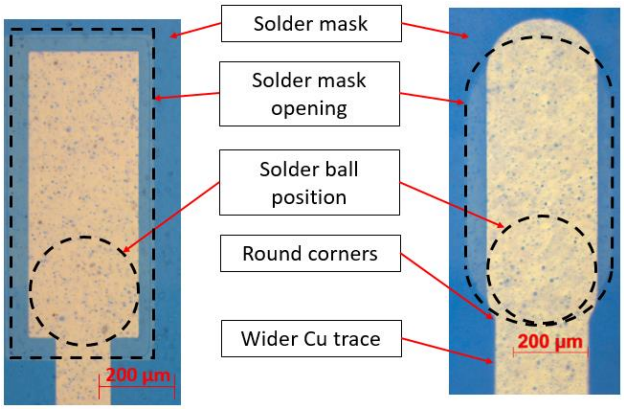

Figure 4. Optical images of the original solder pad design (left) and modified solder pad design (right), obtained using reflection-mode optical microscopy. The modified solder pad design used wider Cu traces, rounded corners and a redesigned solder mask opening that covered the top and bottom part of the solder pad.

This article has been accepted for publication in a future issue of this journal, but has not been fully edited. Content may change prior to final publication. Citation information: DOI 10.1109/TCPMT.2019.2919866, IEEE Transactions on Components, Packaging and Manufacturing Technology

All 20 solder joint locations around the analog front end, AD8232 signal conditioning chip were imaged sequentially, first with the sensor side and then the component side facing the objective lens of an optical microscope. Images were obtained in both reflection and transmission modes (Figure 5a-d) before any TVs were bend tested. In this way, any possible defects that were the result of the assembly process could be detected and imaged. This established a baseline set of images prior to any bend testing. Although the solder pad locations around the signal conditioning chip were imaged with the component side facing the objective lens, the images were not very helpful in spotting defects. Hence, only images taken with the sensor side facing the objective lens were used to evaluate Cu circuit performance.

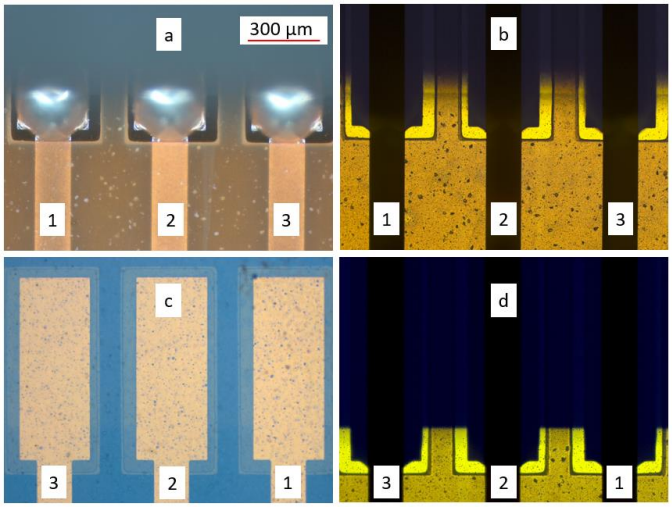

Figure 5. Images of solder joint and pads with the component side facing the objective lens of an optical microscope in reflection (a) and transmission mode (against bright backlight) (b) and as seen through the Kapton® PI substrate in reflection (c) and transmission mode (d) with sensor side facing the objective lens of the optical microscope.

All TVs were bend tested using an Associated Environmental Systems (Model No. BHK 4108) environmental bend tester (Figure 6a). Bend testing was done in two formats. First, the samples were tested with the deflection mandrel pushing against the sensor side (Figure 6b), thereby placing the sensor side in compression and component side in tension, and then against the component side (Figure 6c) to reverse the direction of the bending and the tensile/compressive forces. The first set of TVs was subjected to bend testing with a 4" radius of curvature mandrel pushing against the sensor side for 1000 cycles. The 20 locations around the AD8232 chip were then examined under the optical microscope for new defects. Images were retaken, and the formations of new defects were identified by comparison to the baseline set of images. The process was repeated with 3", 2", 1" and 0.5" radius of curvature mandrels pushing against the sensor side for 1000 cycles each. Similar 1000 cycle tests were done with the mandrel pushing against the component side with 2" and 1" radius of curvature mandrels. For the second set of TVs, 1000 cycle bend testing was done with 2" and 1" radius of curvature mandrels pushing against the sensor side first, and then against the component side. It is notable that due to its size and obvious interference in the bend testing the coin cell battery holder was not present.

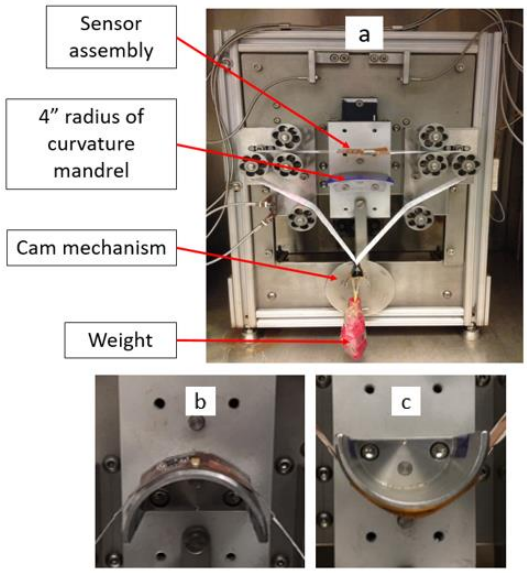

Figure 6. Bend testing set-up (a), mandrel pushing TV against the sensor side (b) and component side (c).

Because the pitch of the AD8232 chip's pin connectors was very small and the solder mask covered the circuit traces around the chip, power-on electrical testing of the TVs was not attempted. Therefore, failure analysis of the Cu circuitry was done only using optical microscopy. After bend testing, cross-sectioning was also done at select joint locations to further characterize the nature of the visually observable defects and failures.

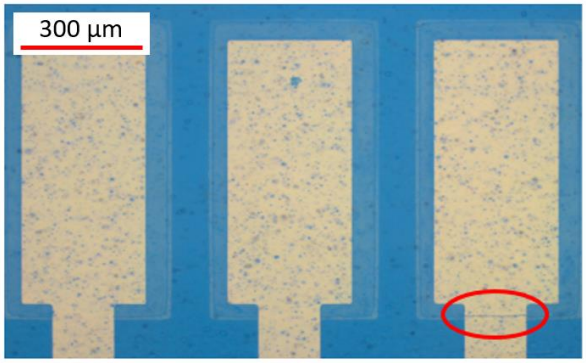

Figure 7. Pristine solder pads (left and middle), and solder pad with a defect (right) in TV 1 (6 µm Cu, 50 µm PI substrate and Sn-Pb solder) before bend testing as seen in reflection mode with sensor side towards the objective lens.

The solder pad locations around the AD8232 chip were imaged before any bend testing was done. In some TVs, defects were observed in this reference set of images (obtained after components were solder attached), indicating that some defects were generated by the thermal cycling of the soldering process alone. One such defect can be seen in Figure 7, as a line defect at the solder pad/trace connection. The nature and severity of such defects have been discussed in more detail below. In the first set of TVs, only TV 5 and 6, which used 6 µm thick Cu traces, 50 µm thick PI substrate and Sn-Bi solder, had zero defects at all 20 solder joints. All other TVs had defects at multiple solder pad locations that were most likely due to thermal stresses incurred during the assembly process. TVs 3, 4, 9, and 10 had defects in more than 15 solder pad locations and were not deemed usable for bend testing.

This article has been accepted for publication in a future issue of this journal, but has not been fully edited. Content may change prior to final publication. Citation information: DOI 10.1109/TCPMT.2019.2919866, IEEE Transactions on Components, Packaging and Manufacturing Technology

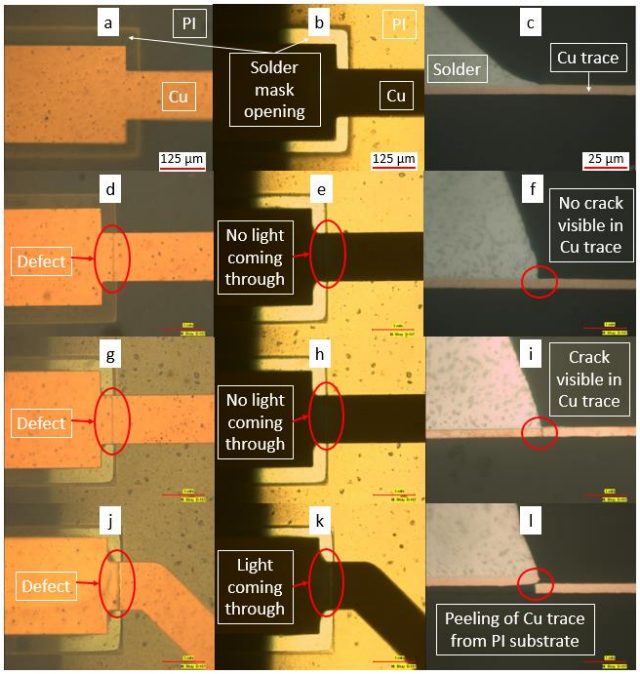

Figure 8. Optical microscopy and cross-section analysis of defects. Pristine solder pad location (a-c). Defect at a solder pad due to local delamination or crack initiation at Cr/PI interface. No through crack can be seen in cross-section, nor is any light seen coming through Cu trace (d-f). Crack through the Cu trace at a solder pad defect location can be seen, indicating worsening of the crack initiation. No light is seen coming through the trace at this point (g-i). Peeling of the Cu trace from the PI substrate indicating total failure of Cu trace. Light can be seen coming through the trace during microscopy in transmission mode (j-l).

The remaining TVs were subjected to bend testing as described previously. All TVs showed new defects developing as the testing progressed, and all the TV material/design combinations were tested to failure. Studying the cross-sections at the defect locations revealed that the defects were of two types and could be readily differentiated using optical microscopy. Type I) Local delamination in the Cr/PI interface or crack in Cu trace and, Type II) Peeling of the Cr/Cu trace from the PI substrate. Figure 8a-c shows a solder pad location in pristine condition with no defect in the Cu solder pad. Figure 8d-f shows a defect as seen in the reflection mode image, but with no visible crack in the transmission mode nor in the cross-section image. This might indicate that there is a local delamination/crack initiation at the Cr/PI interface. The device should be still functional at this stage if all defects in the device are of similar severity. There is no indication of a surface crack in the cross-section image. This local delamination might lead to a crack as seen in Figure 8g-i. At a location where a defect is observed in the reflected light imaging mode (Figure 8g), a visible crack can be seen in Figure 8i. This kind of defect may create an electrical open and there is a chance of device failure. It must be noted that defects seen in Figure 8d–f and in Figure 8g–i looked identical under an optical microscope, and hence have been characterized as Type I defects. When the device continues to be bend tested after the Cu trace through crack as seen in Figure 8i, the flexible substrate bends right at the edge of the rigid solder ball. The stress created due to bend testing is no longer distributed by the Cu traces over a larger area due to the physical disconnect created by the through crack. Due to this, stress is concentrated at the interface of the flexible PI substrate and the Cu solder pad/solder ball which leads to peeling of the solder pad from the PI substrate as seen in Figure 8j-l. Notice that in this case light can be seen coming through the Cu trace in the transmitted light imaging mode, which was not the case in the previous images. Cross-section image Figure 8l clearly shows the Cu trace with a through crack, peeling off the PI substrate, i.e. a Type II defect. Type II defect will definitely create an electrical open leading to device failure. It must be noted that Figure 8 is composed of images taken from multiple TVs showing defects of different intensities. Figure 8a-c are taken from a TV with zero bend cycles and hence no defects are seen. Figure 8d-l are taken from TVs that have undergone complete bend testing (7000 cumulative bend cycles) for set 1 TVs.

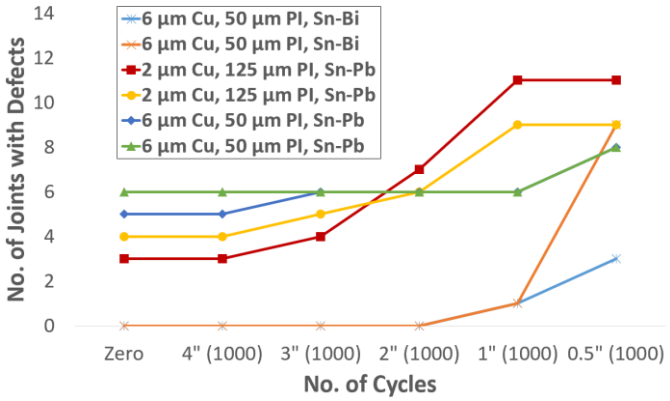

Figure 9. Bend testing results for the first set of TVs with the mandrel pushing against the sensor side showing the occurrence of new Type I defects.

Figure 8 illustrates the progression of damage that can take place at the solder pad locations due to bend testing. Using image data taken before bend testing and comparison of the damage induced through bend testing, we determined the least defect producing and most robust combination of Cu trace thickness, PI thickness and type of solder. It was seen that TVs 5 and 6 using 6 µm Cu, 50 µm PI substrate and Sn-Bi solder, had zero defects after the assembly process, and performed the best (exhibited the least damage) during bend testing. For these samples, the first defect was not observed until after 4000 cumulative cycles with the mandrel pushing against the sensor side and was visible after testing only on the 1” and 0.5” mandrels (Figure 9).

All other TVs showed new defects at an earlier stage in the bend cycling. It must be noted that all the new defects that developed with the mandrel pushing against the sensor side were Type I defects, where a local delamination or crack/crack-initiation could be seen under reflection mode imaging. However, light could not be seen passing through the Cu trace in backlit transmission mode indicating that the Cu trace was not broken and peeling off the substrate. It is likely, however, that these defects produced increased trace resistance and/or intermittent open circuits especially when flexed as they could have had cracks to various degrees in the Cu trace. Type II defects in which the Cu trace breaks and begins to peel were only seen after testing with the mandrel pushing against the component side (Table 2). No new Type I defects were seen during bend testing with mandrel pushing against the component side. As mentioned in the literature review, flexible

This article has been accepted for publication in a future issue of this journal, but has not been fully edited. Content may change prior to final publication. Citation information: DOI 10.1109/TCPMT.2019.2919866, IEEE Transactions on Components, Packaging and Manufacturing Technology

electronics have a highly non-linear response to external loads [26]. The non-linearity of this response might not be the same across samples. Handling of these samples is also not exactly the same across samples. This explains why devices with similar configuration might show a different response to bend testing.

TABLE 2
BEND TESTING RESULTS FOR THE FIRST SET OF TVs WITH MANDREL PUSHING AGAINST THE COMPONENT SIDE SHOWING OCCURRENCE OF TYPE II DEFECTS

TV No.	Configuration	Type II defects after 1000 cycles with 2“ mandrel	Type II defects after 1000 cycles with 1” mandrel
1	6 µm Cu, 50 µm Kapton®, Sn-Pb	0	0
2	6 µm Cu, 50 µm Kapton®, Sn-Pb	0	2
5	6 µm Cu, 50 µm Kapton®, Sn-Bi	0	0
6	6 µm Cu, 50 µm Kapton®, Sn-Bi	0	3
7	2 µm Cu, 125 µm Kapton®, Sn-Pb	0	1
8	2 µm Cu, 125 µm Kapton®, Sn-Pb	1	1
9	2 µm Cu, 125 µm Kapton®, Sn-Bi	0	1
10	2 µm Cu, 125 µm Kapton®, Sn-Bi	1	2

It is notable that Type II defects at each location were always preceded by a Type I defect, indicating a progression toward a circuit open that begins with a crack initiation and concludes with the formation of a fatigue crack across the Cu circuit line. Hence, it is very important to manufacture devices with zero Type I defects after the assembly process, and to ensure that probability of formation of Type I defects due to handling and bending is minimized. It was observed that this probability was minimized by the conditions and materials used for manufacturing TV 5 and 6, i.e. Sn-Bi solder, 6 µm Cu, and 50 µm thick Kapton® HN PI.

The second set of TVs tested the new solder pad design. 4 TVs were fabricated using Sn-Pb solder and 9 devices were fabricated using Sn-Bi solder. Optical inspection of the solder joints revealed that only three TVs, all with lower reflow temperature Sn-Bi solder, had zero Type I or II defects after the assembly process (Figure 10). After the first 1000 cycles of bend testing with a 2" mandrel pushing against the sensor side, none of the TVs with new solder pad design developed new Type I defects for both reflow temperatures. This is an important result since the Gen. 1 HPMs [17] developed cracks in Cu traces near the solder pad location with minimal handling, indicating that the new and improved solder pad design increases the robustness of the devices (Figure 10). New Type I defects were seen after further bend testing with the mandrel pushing against both sensor as well as the component side. However, no Type II defect was seen which was commonly observed in the Gen. 1 HPMs as evident in Figure 2.

Two devices in the first set of TVs and 3 devices in the second set of TVs, which had zero Type I defects as a result of assembly, all used Sn-Bi solder. This indicates that the lower reflow temperature results in less thermal stress due to the coefficient of thermal expansion mismatches, which in turn decreases the chance of generating Type I defects post component-assembly. This offers evidence that crack formation and electrically open circuits result from the cumulative effects of both thermal and mechanical stress and that minimization of both stresses is extremely important to ensure the electrical reliability of FHE devices in real-world use.

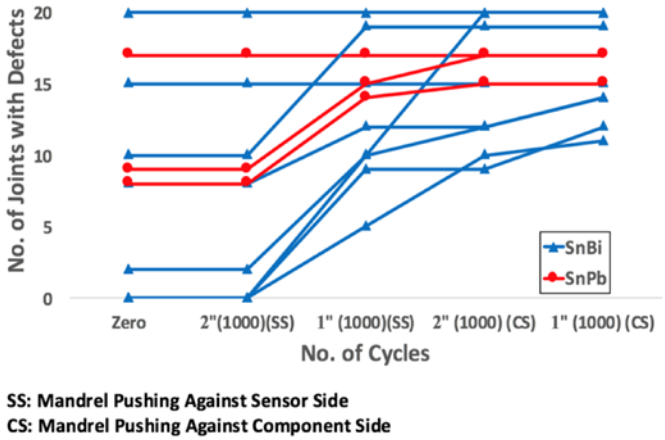

Figure 10. Bend testing results for the second set of TVs with the mandrel pushing against the sensor and component sides. Testing with the mandrel against the component side always followed the sensor side testing.

In the first set of TVs, devices with 6 µm thick Cu circuitry performed better than those with 2 µm thick Cu circuitry. New Type I defects were observed to form more slowly (after a higher number of bend cycles) as compared to devices with 2 µm thick Cu circuitry. This can be attributed to the ability of the thicker Cu circuitry to endure higher bending stresses. This may be due to the thickness of the Cu offering more rigidity and thus spreading the strain over a larger arc during bending, or simply that more cycles are required to initiate a crack in a thicker Cu cross-section. In the second set of TVs, no new Type I defects were seen after 1000 cycles with a 2” radius of curvature mandrel in any of the devices despite having 2 µm thick Cu circuit and 50 µm thick PI substrate. This indicates that the redesigned circuit lines and solder pad improve the reliability of the Cu circuit under bending loads. These findings in terms of the design, materials, and fabrication are very important, which will aid in manufacturing reliable HPMs for large-scale implementation.

B. Printed Au features and Au/metal interfaces

We previously reported [16] that to achieve favorable printing performance and adhesion of our nanoparticle Au ink on Kapton® HN substrate, a plasma surface treatment sequence was required that modified the surface energy of the Kapton®-HN PI. This allowed the ink to wet to the PI surface in such a manner that the ink would maintain it’s as-printed dimensions without beading-up or flowing-out. As in the previous work, no reliability issues were observed for Au ink/Kapton®-HN PI interface.

This article has been accepted for publication in a future issue of this journal, but has not been fully edited. Content may change prior to final publication. Citation information: DOI 10.1109/TCPMT.2019.2919866, IEEE Transactions on Components, Packaging and Manufacturing Technology

A reliability issue involving the printed Au to plated Cu interface in the original HPM hindered the electrical reliability of the devices. The Gen. 1 HPM had two printed Au ECG electrodes. They were electrically connected to plated Cu circuits, on which rigid electronic components were surface mounted using solder reflow. The Au circuits were formed by printing continuous Au traces on the PI substrate that also overlapped onto Cu circuit pads to make electrical connections between the printed sensors and the rigid electronic devices. To create a robust interface between the Au ink and the plated Cu, the printed Au layer needed to have a uniform as-printed thickness, which is maintained until the ink was fully sintered to metallic Au. This requires that the Au ink exhibit favorable wetting and maintain good adhesion to the plated Cu pads. However, three issues arose that compromised the printed Au to Cu interface. 1) Thinning of the printed Au ink occurred as it approached a Cu pad and transitioned up onto it. This occurred immediately after printing and during the sintering, which vaporized the solvent and allowed the Au nanoparticles to coalesce. We observed that the ink wicked from the PI onto the adjacent Cu pad due to the higher surface energy of the Cu compared to that of the PI surface. The resulting excess of ink on the Cu pad resulted in the formation of cracks associated with solvent loss and shrinkage of the ink during drying and curing. 2) The thick uncured ink on the pads remained fluidic until an adequate solvent loss occurred that prevented flow. Until then, gravity-driven movement of the ink on the Cu pads was observed as the parts were transferred into the curing oven. This gave rise to areas of very thick and very thin ink on the Cu pads. The thinner Au ink regions of the Cu pads could also have been more susceptible to oxygen penetration during thermal cures and the formation of Cu oxide at the Au/Cu interface that could degrade adhesion. The thicker regions showed cracks formed during curing that were large fissures down to the Cu pads. 3) Where the ink was wicked from the circuit line adjacent to the Cu pad, the line narrowed substantially, and in some cases, an open was formed. Therefore, a solution for controlling the thickness uniformity of the ink on the Cu pads was needed.

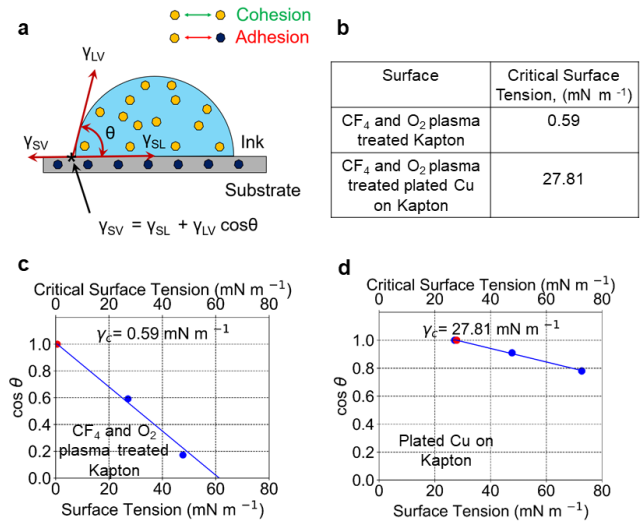

Surface	Critical Surface Tension, (mN m $^{-1}$)
CF_4 and O_2 plasma treated Kapton	0.59
CF_4 and O_2 plasma treated plated Cu on Kapton	27.81

Figure 11. Critical surface tension characterization for various surfaces. (a) Relevant forces expressed by Young's equation when a liquid drop is placed on a solid surface. (b) Summary table of critical surface tensions for the surfaces. (c-d) Zisman plots for determining critical surface tension of (c) O_2 and CF_4 treated Kapton®, and (d) Cu on Kapton® after CF_4 and O_2 plasma treatments.

To understand wetting and spreading of the nanoparticle ink, the surface energy of the surfaces was measured indirectly using a goniometer and contact angle measurements. When a drop of liquid is placed on a solid surface, the drop experiences adhesive forces between the liquid and the solid surface, which favor spreading of the liquid, whereas the cohesive forces within the droplet counteract the spreading. The balance of the forces yields a contact angle, θ as shown in Figure 11a. Young's equation relates the forces in play to the surface free energies of the solid (S), liquid (L), and vapor (V) phases, as shown at the bottom of Figure 11a. For determining the critical surface tension, a series of liquids with decreasing surface tension - hexadecane, ethylene glycol, and deionized water were placed on the solid surface. The receding surface tensions of the liquids help to create an extrapolated line, and at $cos\theta = 1$, the plot yields the critical surface tension of the solid (Figure 11c-d). We characterized the surface tensions of: (i) O_2 and CF_4 plasma treated Kapton®-HN PI and (ii) plated Cu on Kapton®-HN PI after CF_4 and O_2 plasma treatments (Table in Figure 11b). It is apparent that the plated Cu surface demonstrated

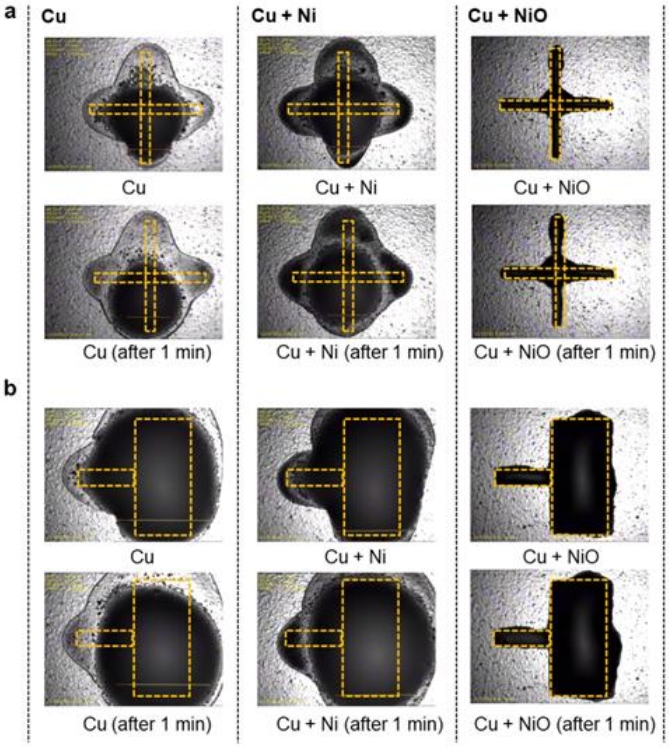

Figure 12. Nanoparticle ink wetting and spreading tests on different metallic surfaces. (a) 1mm x 1mm printed cross and (b) 1mm long and 500 µm wide printed tab on different metallic surfaces. The yellow dotted lines show the intended feature shape. In both (a) and (b), the top panel shows feature definition right after printing, while the bottom panel shows feature definition 1 min after printing. The first column in (a) and (b) shows printing on Cu. The second column in (a) and (b) shows ink spreading on a Ni on Cu surface. After a bake at 190 ˚C for 30 min in air, an oxide layer is formed on the top of the Ni surface which restricts ink spreading to the metal feature. The third column shows printed ink on this oxide surface. The pattern fidelity of printed features on the oxidized surface demonstrates significant improvement over the bare Ni on Cu surface.

This article has been accepted for publication in a future issue of this journal, but has not been fully edited. Content may change prior to final publication. Citation information: DOI 10.1109/TCPMT.2019.2919866, IEEE Transactions on Components, Packaging and Manufacturing Technology

much higher critical surface tension than the PI. Therefore, significant ink spreading is expected on this surface.

To study the printed Au line thinning, a series of experiments were performed on different metallic surfaces. These surfaces went through CF_4 and O_2 plasma treatments. The plasma treatment conditions are described in our previous work [16]. Figure 12 shows a printed cross and a tab on: (i) Cu, (ii) Cu and nickel (Ni) and (iii) Cu and oxidized Ni. The cross and the tab on the metallic surfaces show significant spreading. These results are aligned with the findings from the critical surface tension studies, where the metallic surfaces had significantly higher critical surface tension than CF_4 and O_2 plasma treated Kapton® HN PI. As a result, the nanoparticle ink spreading is greater on the metallic surfaces than on CF_4 and O_2 plasma treated Kapton® HN PI. A conclusion can be drawn from these tests that a subsequent surface treatment is required for the metallic surfaces to restrict ink spreading. While the base Ni surface was conducive to ink spreading, oxidizing the surface in air at 190 ˚C for 30 min drastically improved printability (Figure 12, third column). The oxide layer demonstrates lower critical surface tension compared to a bare Ni surface, which restricted the ink spreading. These results are shown in Figure 12. The first column shows printing on Cu on Kapton® HN PI after CF_4 and O_2 plasma treatments. The cross and the tab did not hold their shape. Yellow dotted lines show the intended feature. Ink spreading on a Ni on Cu surface is shown in the second column. Here too, considerable spreading of the ink hinders the pattern formation. Oxidizing the surface in air improved the printability of the surface, which is clear from the printed cross and the tab in the third column of Figure 12. Therefore, utilizing nickel oxide (NiO) dams can restrict ink spreading.

One of the electrical failure mechanisms for the original HPM [17] was an interfacial separation of printed Au from the plated Cu pads. This overlap was required for electrical interconnection of the printed sensors to the rigid components. A robust interface between these materials is necessary to preclude interfacial separation during subsequent thermal treatments required for nanoparticle ink and solder mask cures, and to survive flexing-induced mechanical stress during use. Interfacial failure at the Au/Cu interface was observed to result in either partial loss (increased resistance) or total loss of electrical connections (opens) in the circuit. After studying the wetting and spreading of the nanoparticle ink on various surfaces, a TV was built comprised of daisy chains of plated 3 µm thick Cu pads and interconnecting printed Au features. This design is shown in Figure 13a. The Cu features were first pattern-plated on the Kapton® HN PI. Four types of surfaces were then prepared using the base plated Cu surface. i) Bare plated Cu, ii) plated Cu with NiO layer, iii) plated Cu with plated 250 nm thick Au layer, and iv) plated Cu with plated 250 nm thick Au layer with NiO layer on top. The electroplated Au layer was deposited using a potassium gold cyanide bath. Then, lines of Au ink were printed to interconnect plated Cu pads forming multiple arrays of Cu interconnected by printed Au circuit lines. Referring to Figure 13a, this created three continuous electrically testable metallic serpentines of different lengths. This TV was used to test the four different metal pad surfaces, with the first goal to control printed Au ink flow, and

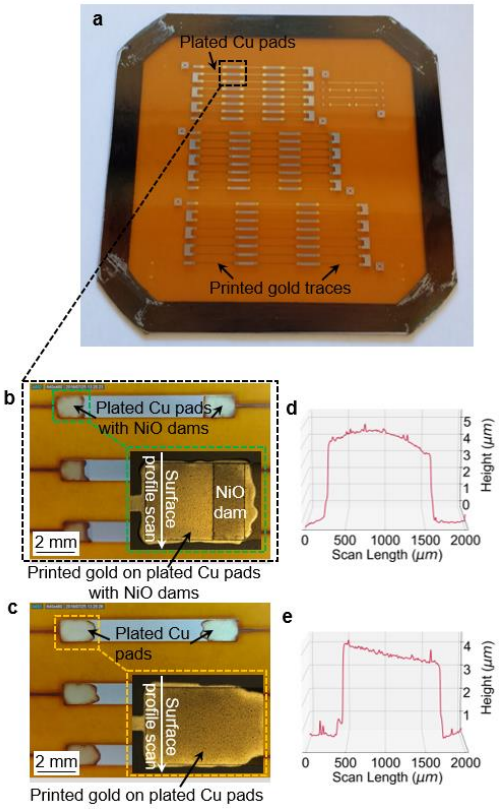

Figure 13. Printing reliability improvement TV and the use of NiO dams. (a) The printing TV after all metallization and printing has been completed. The Cu pads were interconnected by printing Au traces between two Cu pads. (b) Pinning of the Au ink at the edge of the NiO dam. Due to the high volume, there was some ink spill over. (c) Ink runout in the case of Cu pads without the NiO dams. The runout resulted in thinning of the ink at the printed Au / plated Cu interface. (d) Surface profile of Au ink printed on Cu pad with NiO dam. (e) Surface profile of Au ink printed on Cu pad without NiO dam. Surface profile measured includes Cu pad thickness of 3 µm.

secondly to learn how to form a more robust adhesive interface between the printed Au ink and plated Cu pads. Additionally, the TV was tested electrically after thermal cycling and bend testing, looking for any change in conductivity that would be indicative of interfacial breakdown. Figures 13b-c show a magnified view of the resultant serpentine pattern after Au printing between the 3 µm thick Cu pads. Printed Au lines were used to interconnect the Cu pads with (Figure 13b) and without (Figure 13c) NiO dams. The NiO dams were tested for their ability to restrict the area of the pad and ink flow off the pad. It was observed that printed Au ink formed a more even layer on Cu pads with NiO dams with a thickness of 1 µm at the center of the pad (Figure 13d). On Cu pads without NiO dams, the printed Au ink formed an uneven layer with a thickness of only 500 nm at the center of the pads (Figure 13e). The NiO dams that act as partial barriers, reduce the area of the Cu pads limiting the volume of the ink wicking from the connected Au circuit lines (Figure 13b). While in Figure 13c, without the NiO dams, the printed ink spreads onto the substrate, resulting in non-uniformity of the printed ink on the Cu pad.

After printing, the TV was subjected to simulated thermal and mechanical stressing followed by electrical testing. Thermal cycles were simulated using reflow profiles of the Sn-Pb solder. Following the thermal stressing and resistance

This article has been accepted for publication in a future issue of this journal, but has not been fully edited. Content may change prior to final publication. Citation information: DOI 10.1109/TCPMT.2019.2919866, IEEE Transactions on Components, Packaging and Manufacturing Technology

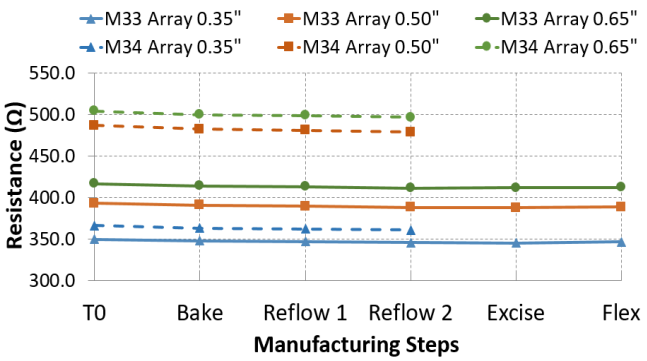

Figure 14. The TV array resistance before and after thermal cycling and flexing. Different manufacturing steps: T0 was immediately after the manufacturing build; bake followed solder mask cure at 150 ˚C for 1 h; reflows 1 and 2 were measured after exposure to a simulated solder reflow at 205 ˚C, and excise was to check for a response after the parts were cut from the substrate tensioned on a frame. Flex was after 1000 bend cycles on a 2" mandrel. Results for 6 arrays are shown, where the length of the arrays (distance between two Cu pads) was varied from 0.35" to 0.65".

measurements, three individual conductive serpentines were excised from each frame. Each serpentine is in a format that can be readily mounted on the bend cycle fatigue tester to see if resistance changes are detected which are indicative of interfacial failure. Bend testing was done for 1000 cycles using a 2" radius of curvature mandrel. The electrical resistance measured is the sum of not only the plated Cu and printed Au conductors, but also any contribution from the Au/Cu interfaces. Figure 14 shows results for the measured DC electrical resistance of the arrays and interfaces before and after exposure to simulated solder reflows and for bend testing. Results of TVs with plated Cu pads with plated Au layer but no NiO layer on top, M33 and M34, are shown. M33 was excised and bend tested, whereas M34 was not. Each array for all 4 surface variations was shown to be stable as a function of all thermal cycles and bend testing. The variation in resistance is mainly due to non-uniformity in the Au ink printing process and can be minimized by fine-tuning the printing parameters. The slight decrease in resistance with increasing thermal exposures

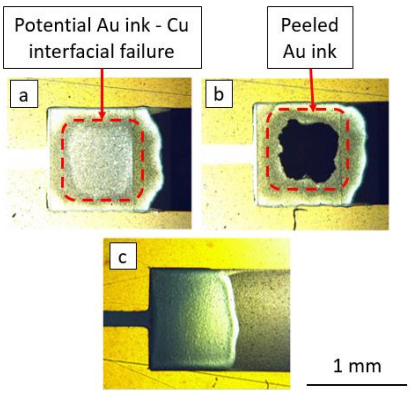

Figure 15. Comparison of Au ink printed on Cu pads without and with gold-plating. Au ink printed on Cu pads without protective Au plating (a). The bright center is indicative of the interfacial failure that worsens with abrasion during flex testing and ultimately results in peeling of the Au ink (b). Au ink printed on Cu pads with Au plating demonstrates good adhesion between the plated Au and the printed Au (c). All images were taken following thermal cycling (a simulated solder mask cure cycle followed by 2x reflow cycles at 205 ˚C peak temperature).

can be attributed to additional sintering of Au nanoparticles by thermal annealing. Similarly, the small increase in resistance after bend testing in M33 traces can be attributed to minor mechanical damage in printed Au. Again, this indicates that the individual traces and interconnects are robust. Thus, these electrodes, traces and interconnects are suitable for application in the HPM.

It is notable that we did observe some blistering and peeling of Au ink on Cu pads following the thermal stresses (Figure 15a-b). During the sintering of the Au ink, formation of Cu oxide at the interface results in the generation of blisters on top of the pad. The interfacial failure between the Cu oxide and the printed gold results in blistering, and eventually delamination. The Cu oxide formation was prevented by plating Cu pads with a thin Ni/Au layer. Au plated Cu pads did not show any delamination as shown in Figure 15c.

III. Improved Generation 2 HPMs

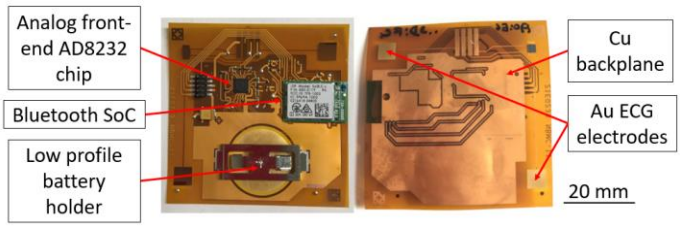

Figure 16. Improved Gen. 2 HPM component side (left) and sensor side (right).

In summary, in the first set of TVs fabricated to improve Cu circuit reliability, only TVs using 6 µm Cu, 50 µm PI and Sn-Bi solder had zero Type I defects after assembly. These were the same TVs that also performed best in bend testing. Bend testing of the second set of TVs that incorporated a new solder pad design indicated that the redesign resulted in further improvement in reliability. While printability of Au nanoparticle ink on plated Cu pads can be significantly improved using a NiO dam, some amount of overflow was also seen beyond the NiO dams which reduced their efficacy. Hence, the most reliable Cu/Au interface was achieved by plating Ni/Au on cleaned, no Cu oxide, Cu surfaces and printing Au ink onto the plated Au.

TABLE 3
COMPARISON OF GEN. 1 AND GEN. 2 HPM SPECIFICATIONS

Parameter	Gen. 1 HPM	Gen. 2 HPM
Solder	Sn-Pb	Sn-Bi
Cu circuit thickness (µm)	2	2 or 6
PI thickness (µm)	50	50
Solder pad design	Original	Improved
ECG electrode fabrication method	Printed Au ink	Printed Au ink or electroplated Au
Au trace to Cu circuit interface	Printed Au trace on bare Cu	Printed Au on Ni/Au plated Cu or plated Au on Ni plated Cu
Battery holder	Thicker battery holder	Low profile battery holder

A total of 21 Generation 2 (Gen. 2) HPMs were fabricated, guided by results from TV testing. These HPMs were fabricated

This article has been accepted for publication in a future issue of this journal, but has not been fully edited. Content may change prior to final publication. Citation information: DOI 10.1109/TCPMT.2019.2919866, IEEE Transactions on Components, Packaging and Manufacturing Technology

using both 2 µm and 6 µm thick Cu circuit on 50 µm thick PI substrates and the improved solder pad design. All components were surface mounted using the lower-reflow temperature Sn-Bi solder. The Cu pads where Au nanoparticle ink traces overlapped to connect Au ECG electrodes to the rigid electronic components were plated with Ni/Au to mitigate Au/Cu delamination. Two subsets of Gen. 2 HPMs were built whereby ECG electrodes were fabricated using printed Au nanoparticle ink (subset 1) as well as electroplated Au on a Cu base layer (subset 2). Electroplated Au electrodes were used because they avoid many printing issues associated with fabricating electrodes using printed Au nanoparticle ink. The Cu ground plane that was present in the Gen. 1 HPM was also retained. However, it was redesigned so that it reinforced regions of high flexibility that would result in an area of high strain. This reinforced the substrate under the analog front-end signal conditioning chip. A low-profile battery holder was used to reduce the overall thickness of the device (Figure 16). Process flow similar to the one used to fabricate Gen. 1 HPMs was used to fabricate Gen. 2 HPMs also. However, while fabricating Gen. 1 HPMs, solder mask was deposited over the Cu circuitization on the component side before Au electrodes were printed on the sensor side. This caused oxidation of Cu under the solder mask during sintering of the Au nanoparticle ink that degraded adhesion between Cu and the solder mask. During fabrication of Gen. 2 HPMs, the solder mask was deposited after printing and sintering or electroplating of the Au traces and electrodes. This allowed for cleaning of the Cu circuitization surface before solder mask deposition which improved adhesion between Cu and solder mask. Table 3 summarizes the difference between Gen. 1 and Gen 2. HPMs.

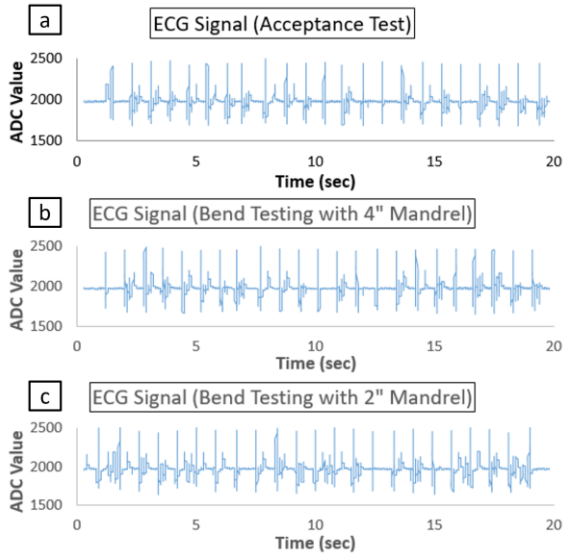

Figure 17. Recorded archived ECG signals from the HPMs as received at the host for the indicated stage of testing. a) as manufactured, i.e., prior to bend testing, b) after bend testing for 500 cycles with a 4" radius of curvature mandrel and c) after bend testing for 500 cycles with a 2" radius of curvature mandrel pushing against the sensor side.

Each HPM was first subjected to functionality testing using archived ECG signals to confirm their operation immediately after fabrication, and to test functionality after encapsulation and bend testing. The HPMs were mounted using a conductive gel to contact the electrodes and skin of human test subjects. The subjects performed moderate exercise until their heart rates reached 60% of the subjects' maximum recommended heart rate. ECG signals were recorded at rest, during exercise, and then again at rest. All human subject tests were conducted in compliance with Binghamton University's Institutional Review Board approved protocol 3267-14. 18 of 21 HPMs passed initial archive and human subject testing and were encapsulated with AI Technology PN CC7130-PR encapsulant applied with a paintbrush to protect the component side from moisture. Three failed due to cracks or lack of adhesion of printed Au traces. The entire component side was coated except for the battery holder and battery contact pad. The layer of encapsulant was as thin as possible to minimize altering the flexibility of the device. The HPMs were again checked for functionality using archived ECG signals. Fifteen passed, 2 failed at the connection to the ECG electrodes, and 1 was not encapsulated. Following the second test, eleven devices were subjected to bend testing for 500 cycles using a 4" radius of curvature mandrel pressing against the sensor side. 6 passed the subsequent archived ECG signal test, and 5 failed, 4 due to a break in the electrode trace and 1 due to delamination of the electrode. 6 HPMs were subjected to 500 bending cycles on a 2" mandrel pressing against the sensor side, and all passed the subsequent archive signal test. Seven out of 18 Gen. 2 HPMs tested failed. Six due to a broken trace to at least one ECG electrode and 1 due to electrode delamination. It is important to note that the design of the electrodes, signal traces and solder mask on the sensor side was the same as the Gen. 1 HPMs. Thus, applying the design changes of the Gen. 2 Cu circuitization to the Au sensor and trace design is expected to significantly improve their robustness (Table 4 and Figure 17).

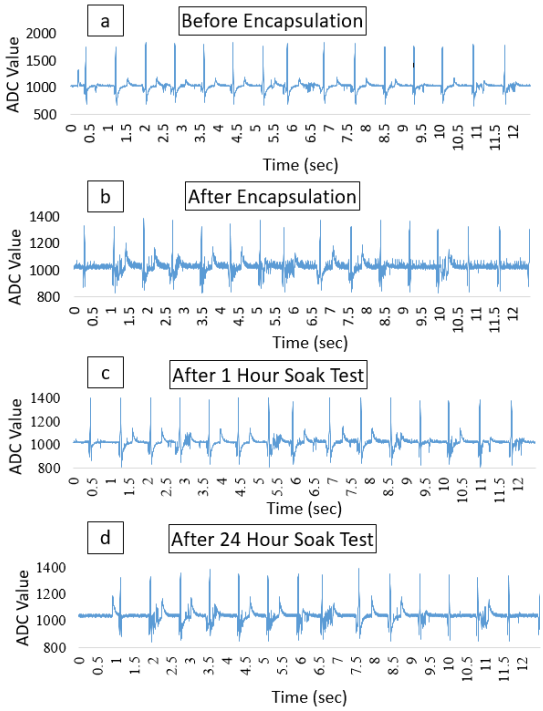

Figure 18. Archived ECG signals recorded from a HPM before encapsulation (a), after encapsulation (b), after the 1 h soak test (c) and 24 h soak test (d).

In real-world use, the devices will be in intimate skin contact and exposed to the perspiration of the wearer. This exposure to water and salts could cause electronic components on the

This article has been accepted for publication in a future issue of this journal, but has not been fully edited. Content may change prior to final publication. Citation information: DOI 10.1109/TCPMT.2019.2919866, IEEE Transactions on Components, Packaging and Manufacturing Technology

TABLE 4
GEN. 2 HPM TEST SUMMARY

Device	Cu thickness (μm)	Electrode Type	Acceptance Testing (Archive ECG signals)	Human Subject Testing	Functionality Test Post Encapsulation	Functionality Test After 500 cycles with 4" mandrel	Functionality Test After 500 cycles with 2" mandrel
1	6	Electroplated	Pass	Pass	Pass	Not bend tested	NA
2	6	Electroplated	Pass	Pass	Pass	Pass	Pass
3	6	Electroplated	Pass	Pass	Right Au electrode failure	NA	NA
4	6	Electroplated	Pass	Pass	Not encapsulated	Not bend tested	NA
5	6	Electroplated	Pass	Pass	Pass	Left Au electrode failure	NA
6	6	Electroplated	Pass	Pass	Pass	Not bend tested	NA
7	6	Electroplated	Pass	Pass	Pass	Not bend tested	NA
8	6	Electroplated	Pass	Pass	Pass	Pass	Pass
9	2	Electroplated	Pass	Pass	Pass	Left Au electrode failure	NA
10	2	Electroplated	Pass	Pass	Pass	Pass	Pass
11	2	Electroplated	Pass	Pass	Pass	Not bend tested	NA
12	2	Electroplated	Pass	Pass	Pass	Fail*	NA
13	2	Printed	Pass	Pass	Pass	Pass	Pass
14	2	Printed	Pass	Pass	Both Au electrodes failed	NA	NA
15	2	Printed	Pass	Pass	Pass	Right Au electrode failure	NA
16	2	Printed	Pass	Pass	Pass	Right Au electrode failure	NA
17	2	Printed	Pass	Pass	Pass	Pass	Pass
18	6	Printed	Pass	Pass	Pass	Pass	Pass
19	6	Printed	Failed due to Au nanoparticle ink printing problems				
20	6	Printed	Failed due to Au nanoparticle ink printing problems				
21	6	Printed	Failed due to Au nanoparticle ink printing problems				

*Device failed due to delamination and peeling of Au electrodes.

component side to short causing device failure. To protect the device from this mode of failure, the component side of the HPMs were encapsulated with AI Technology PN CC7130-PR encapsulant. Five HPMs were encapsulated for this test. These were new, previously untested Gen. 2 HPMs and were not part of the set of 21 HPMs used in human subject testing. The devices were tested using archived ECG signal before and after the encapsulation process to ensure both their pre-test and post-test functionality. They were then submerged in a saline solution for 1 h, after which they were rinsed with room temperature tap water and dried overnight. Their functionality was again tested with archived ECG signals. The devices that passed the first round of encapsulation and soak tests were encapsulated with a second coat of encapsulant using the same AI Technology PN CC7130-PR encapsulant or another material as detailed in Table 5. The devices were submerged in a saline solution for 24 h, rinsed, and air dried as described previously. Their functionality was then retested using the same archived ECG signals. Figure 18 shows the archive ECG signals transmitted from a typical device that passed all the tests to determine the barrier effectiveness of the encapsulation against the saline solution.

TABLE 5
SUMMARY OF SOAK TESTS CONDUCTED AT ROOM TEMPERATURE IN NORMAL SALINE SOLUTION FOR 5 GEN. 2 HPMs

Device	Before Encap.	1st layer	1-h test	2nd layer	24-h test
1	Pass	Fail (Did not power up)	NA	NA	NA
2	Pass	Pass	Pass	Waterproof Sealant Loctite Clear Silicone Sealant IDH# 908570	Pass
3	Pass	Pass	Pass	GOOP Amazing GOOP All Purpose Plumbing Product # 1000021	Pass
4	Pass	Pass	Pass	AI Technology PN CC7130-PR	Pass
5	Pass	Pass	Pass	AI Technology PN CC7130-PR (Thicker second coat)	Pass

Table 5 shows that all the devices passed functionality testing before encapsulation, and 4 out of 5 devices passed the functionality test after a first-layer of encapsulation was

applied. This demonstrates that devices can be successfully encapsulated using AI Technology PN CC7130-PR without damaging them. Failure of one device can be attributed to the fact that the devices were encapsulated manually with no prior experience with the material or the method used. All 4 devices that were functional after application of the first layer of encapsulation passed the 1 h soak test. Further, the devices remained functional after encapsulation with a second layer of encapsulant, and also passed a subsequent 24 h soak test. This shows that the materials used for encapsulation provided an effective barrier of protection against sweat, which will keep the devices functional in practical use.

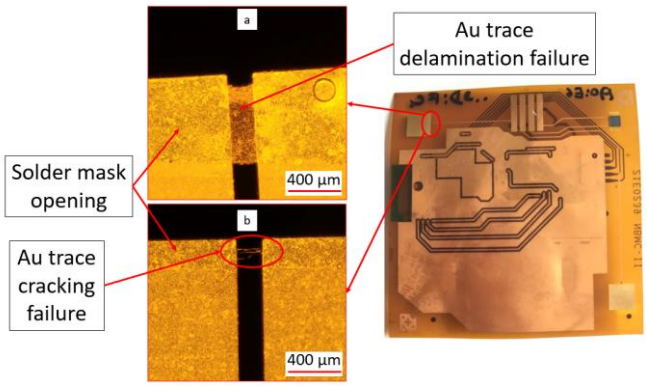

Figure 19. Failure of Au trace (a) due to delamination of the plated Cu/Au circuit from the PI surface and, (b) cracking. a and b show the trace as visible against back lighting in transmission mode so that the crack that is circled is observable.

Device failure in Gen. 2 HPMs that underwent human subject testing was observed during bend testing that followed the encapsulation process. It was seen that the failure of the improved HPMs could be correlated to failure of Au traces near the solder mask openings of the electrodes. The failures were observed at this location in both printed as well as electroplated Au traces. The failures were of two types. i) Delamination of the printed or electroplated Au traces (Figure 19a) or, ii) fracture of the printed or electroplated Au traces that resulted in an electrical open (Figure 19b). In both cases, the failures were seen at the solder mask opening implying that the edge of the solder mask was a locus of strain concentration. This strain may have resulted from residual thermal stress created by solder mask shrinkage during thermal curing and subsequent cool down, or due to the formation of a hinge region where the cross-section rapidly transitions from less flexible (with solder mask present) to more flexible (without solder mask present), or most likely a combination of both. The nature of the cracks in the electroplated electrodes was very similar to cracks in Cu traces observed near the signal conditioning chip. It was observed in TVs with improved solder pad design that covering the top and bottom of the pads with solder mask and rounding the corners of the solder pads and solder mask openings reduced point-stress (and hence strain) concentrations. These design changes substantially decreased the frequency of formation of circuit deformations and cracks, and thus enhanced the durability of the devices during mechanical and thermal stress exposures. We believe a similar design improvement could improve the reliability of the Au electrode/trace junction region as well. It is encouraging that no visible cracks were seen in the encapsulation on any of the tested HPMs after bend testing. In three of the Gen. 2 HPM devices (Table 4), we observed that Au printing issues were still present. The majority of the printing defects could be attributed to improper ink spreading. These are mainly process control issues related to controlling ink volumes and matching the surface energies of the ink, Cu, and PI.

IV. Summary

The original Gen I HPMs, built and tested in our previous work, were susceptible to cracking of the Cu circuit which caused the device to fail [17]. Bend testing of multiple TVs indicated that using a lower reflow temperature solder to mount electronic components (175 ˚C vs. 205 ˚C) on the component side of the device helped reduce the number of Type I defects during assembly. It was also shown that thicker Cu (6um vs. 2um) circuitry is more robust under bend testing. Design changes in the shape of the solder pads and solder mask opening and their placement (partial capture of the pads by the solder mask) decreased the strain concentration at these “hinge” locations (where the cross-section contained the least Cu, or at a pad edge where thick rigid solder on a pad transitions to a thinner much more flexible cross-section). These changes were found to increase the robustness of joint locations under bending load.

There were also issues with the printing of Au nanoparticle ink in the Gen. 1 HPM. With the surface energy of the PI substrate adjusted using CF_4 and O_2 plasma treatments to optimize Au ink printing on PI, it was observed that ink overlapping on Cu pads would thin out due to excessive spreading. While we found some success using NiO as a barrier layer to limit spreading, the key factor that determined pad finish metallurgy was the prevention of Cu corrosion from thermal treatments (cures and reflow). This was achieved by over plating the Cu solder pads selectively with Ni/Au. Significant improvement in the reliability of the Cu/ink interface was seen using this method. Ink spreading on the pads and subsequent wicking of ink from the connecting printed circuit lines was best controlled by decreasing the solder pad sizes and simply controlling the printing parameters and adjusting printed ink volume. TVs demonstrated robust endurance on the PI when exposed to both thermal as well as mechanical stress testing.

Improved, fully functional Gen. 2 HPMs were fabricated by incorporating learnings from the testing of TVs fabricated as non-functional partial devices that separately assessed improvements in the reliability of Cu circuitry and the printed Au nanoparticle ink. Improved Gen. 2 HPMs were also fabricated using electroplated (Ni/Au on Cu) ECG sensor electrodes. The devices showed improvement in reliability over the Gen. 1 HPMs which used printed Au electrodes formed from Au-precursor nanoparticle ink. Recordings from the two types of electrodes were indistinguishable. It was also found that the devices could be effectively encapsulated to protect them from saline solution exposure, a reasonable representation of human perspiration. Despite these improvements, there is certainly more work to do to fully assess the reliability of Au electrodes, both printed and electroplated. It must be noted that

both Gen. 1 and Gen. 2 devices had a Cu backplane which will have an effect on device reliability. However, in this study, the focus was on improving the reliability of the Cu circuit only. Since Cu backplane is present in both generations of devices, improving reliability of Cu circuit will improve overall reliability of the device.

The experimental work done in this study, though immensely helpful, was time and resource consuming, which increased the design cycle time. Finite element analysis can be used to predict stresses in different design configurations which can reduce the design cycle time. We conducted a feasibility study on stress analysis of Cu circuit for this human performance monitor and found that simulation results correlated closely with experimental results [18]. Hence, finite element analysis can be employed in similar future studies.

The device currently uses rigid components for signal conditioning and communication purposes. Flexible electronic components would be preferred, to improve reliability under bending loads by the elimination of strain concentrations that are associated with small bend radii. Flexible components have the advantage in that they can bend with the substrate. A flexible operational amplifier developed by American Semiconductor, Inc. is presently being used as a test vehicle to define preliminary best practices for mounting this device on our flexible substrate [29]. The electrodes that were used in this study required the use of a conductive gel to establish contact with the skin of the human subject. This configuration is not very desirable as ECG detection requires that the gel remains in place and it leaves a gel residue on the skin upon removal of the device. We are currently investigating the use of capacitive coupled electrodes instead of contact-based electrodes to eliminate the conductive gel. Another limitation of truly wireless flexible hybrid electronic devices is its battery life. Such devices often employ Bluetooth technology for communication purposes which can be very power intensive. Battery life of these devices can be improved by using lower power electronic component and transmitting data more efficiently. This can be further complemented by use of energy harvesting technology [30]. These developments will prove to be very important stepping stones in the development of FHE devices for both professional healthcare and amateur fitness monitoring.

ACKNOWLEDGMENT

This work was primarily funded by contract # FA86501327311-7 from the NanoBio Manufacturing Consortium through a program sponsored by the Air Force Research Laboratory. This material is also based, in part, on research sponsored by Air Force Research Laboratory under agreement number FA8650-15-2-5401 via FlexTech Alliance, Inc., as conducted through its flexible hybrid electronics manufacturing innovation institute. The U.S. Government is authorized to reproduce and distribute reprints for governmental purposes notwithstanding any copyright notation thereon. The fabrication of the Gen. 1 and Gen. 2 HPM devices as well as all the TVs, except the Au nanoparticle ink printing, was done at i3 Electronic, Inc. in Endicott, NY. The printing of Au nanoparticle ink sensors and traces on all devices and TVs was done at University of California at Berkeley, Berkeley, CA. The mechanical bend testing of all the devices and TVs was done at Binghamton University, Binghamton, NY.

REFERENCES

[1] Yan Wang, Li Wang, Tingting Yang, Xiao Li, Xiaobei Zang, Miao Zhu, Kunlin Wang, Dehai Wu and Hongwei Zhu. “Wearable and highly sensitive graphene strain sensors for human motion monitoring.” *Advanced Functional Materials*, Vol. 24, No. 29, pp. 4666-4670, 2014.

[2] Gregor Schwartz, Benjamin C-K. Tee, Jianguo Mei, Anthony L. Appleton, Do Hwan Kim, Huiliang Wang and Zhenan Bao. “Flexible polymer transistors with high pressure sensitivity for application in electronic skin and health monitoring.” *Nature communications*, Vol. 4, pp. 1859, 2013.

[3] Amay J. Bandodkar, Denise Molinnus, Omar Mirza, Tomás Guinovart, Joshua R. Windmiller, Gabriela Valdés-Ramírez, Francisco J. Andrade, Michael J. Schöning and Joseph Wang. “Epidermal tattoo potentiometric sodium sensors with wireless signal transduction for continuous non-invasive sweat monitoring.” *Biosensors and bioelectronics*, Vol. 54, pp. 603-609, 2014.

[4] Daniel P. Rose, Michael E. Ratterman, Daniel K. Griffin, Linlin Hou, Nancy Kelley-Loughnane, Rajesh R. Naik, Joshua A. Hagen, Ian Papautsky and Jason C. Heikenfeld. “Adhesive RFID sensor patch for monitoring of sweat electrolytes.” *IEEE Transactions on Biomedical Engineering, Vol.* 62, No. 6, pp. 1457-1465, 2015.

[5] Taehoon Kim, Junyong Park, Jongmoo Sohn, Donghwi Cho and Seokwoo Jeon. “Bioinspired, highly stretchable, and conductive dry adhesives based on 1D–2D hybrid carbon nanocomposites for all-in-one ECG electrodes.” *ACS nano, Vol.* 10, No. 4, pp. 4770-4778, 2016.

[6] Sarah L. Swisher, Monica C. Lin, Amy Liao, Elisabeth J. Leeflang, Yasser Khan, Felippe J. Pavinatto, Kaylee Mann et al. “Impedance sensing device enables early detection of pressure ulcers in vivo.” *Nature communications* 6, 2015.

[7] Yasser Khan, Aminy E. Ostfeld, Claire M. Lochner, Adrien Pierre and Ana C. Arias. “Monitoring of vital signs with flexible and wearable medical devices.” *Advanced Materials, Vol.* 28, No. 22, pp. 4373-4395, 2016.

[8] D. Yamamoto, S. Nakata, K. Kanao, T. Arie, S. Akita and K. Takei. "All-printed, planar-type multi-functional wearable flexible patch integrated with acceleration, temperature, and ECG sensors." In *2017 IEEE 30th International Conference on Micro Electro Mechanical Systems (MEMS)*, Las Vegas, Nevada, USA, Jan. 22nd – 26th, pp. 239-242, 2017.

[9] Ningqi Luo, Wenxuan Dai, Chenglin Li, Zhiqiang Zhou, Liyuan Lu, Carmen CY Poon, Shih-Chi Chen, Yuanting Zhang and Ni Zhao. "Flexible piezoresistive sensor patch enabling ultralow power cuffless blood pressure measurement." *Advanced Functional Materials, Vol.* 26, No. 8, pp. 1178-1187, 2016.

[10] Yuki Yamamoto, Shingo Harada, Daisuke Yamamoto, Wataru Honda, Takayuki Arie, Seiji Akita and Kuniharu Takei. "Printed multifunctional flexible device with an integrated motion sensor for health care monitoring." *Science Advances*, Vol. 2, No. 11, e1601473, 2016.

[11] Ha-Chul Jung, Jin-Hee Moon, Dong-Hyun Baek, Jae-Hee Lee, Yoon-Young Choi, Joung-Sook Hong and Sang-Hoon Lee. "CNT/PDMS composite flexible dry electrodes for long-term ECG monitoring." *IEEE Transactions on Biomedical Engineering*, Vol. 59, No. 5, pp. 1472-1479, 2012.

[12] Jeong Su Lee, Jeong Heo, Won Kyu Lee, Yong Gyu Lim, Youn Ho Kim and Kwang Suk Park. "Flexible capacitive electrodes for minimizing motion artifacts in ambulatory electrocardiograms." *Sensors* Vol. 14, No. 8, pp. 14732-14743, 2014.

[13] Ebrahim Nemati, M. Jamal Deen and Tapas Mondal. "A wireless wearable ECG sensor for long-term applications." *IEEE Communications Magazine*, Vol. 50, No. 1, pp. 36-43, 2012.

[14] S. Asif Hussain, Ajay Vikram Singh, Chandra Shekar Ramaiah and S. Javeed Hussain. "A wireless device for patient ECG monitoring and motion activity recording for medical applications." In *2016 5th International Conference on Reliability, Infocom Technologies and Optimization (Trends and Future Directions) (ICRITO)*, Noida, India, Sept 7th–9th, pp. 634-641, 2016.

[15] Chacko John Deepu, X. Zhang, W-S. Liew, David Liang Tai Wong and Yong Lian. "Live demonstration: An ECG-on-chip for wearable wireless sensors." In *2014 IEEE Asia Pacific Conference on Circuits and Systems (APCCAS)*, Ishigaki, Japan, Nov. 17th-20th, pp. 177-178. 2014.

[16] Yasser Khan, Mohit Garg, Qiong Gui, Mark Schadt, Abhinav Gaikwad, Donggeon Han, Natasha AD Yamamoto et al. "Flexible Hybrid Electronics: Direct Interfacing of Soft and Hard Electronics for Wearable Health Monitoring." *Advanced Functional Materials*, Vol. 26, No. 47, pp. 8764-8775, 2016.

[17] Mark Poliks, James Turner, Kanad Ghose, Zhanpeng Jin, Mohit Garg, Qiong Gui, Ana Arias, Yasser Kahn, Mark Schadt and Frank Egitto. "A Wearable Flexible Hybrid Electronics ECG Monitor." In Proceedings of the 2016 IEEE 66th *Electronic Components and Technology Conference (ECTC)*, Las Vegas, Nevada, May 31 – June 3, pp. 1623-1631, 2016.

[18] Varun Soman, Mark D. Poliks, James N. Turner, Mark Schadt, Michael Shay, Frank Egitto. "Reliability Study and Finite Element Modeling of a Wearable Sensor Patch (WSP) to Monitor ECG Signals." In Proceedings of the 2018 IEEE 66th *Electronic Components and Technology Conference (ECTC)*, San Diego, California, May 29th – June 1st, pp. 1865-1872, 2018.

[19] Varun Soman, Mark D. Poliks, James N. Turner, Mark Schadt, Michael Shay and Frank Egitto. "Reliability Analysis of a Wearable Sensor Patch (WSP) to Monitor ECG Signals." In *International Microelectronics Assembly and Packaging Society 2017 International Symposium on Microelectronics*, Raleigh, NC, USA, Oct 9th-12th, pp. 194-200, 2017.

[20] J. Reboun, S. Pretl, J. Navratil and J. Hlina. "Bending endurance of printed conductive patterns on flexible substrates." Proceedings of the *2016 IEEE 39th International Spring Seminar on Electronics Technology (ISSE)*, Pilsen, Czech Republic, May 18 - 22, pp. 184-188, 2016.

[21] Eerik Halonen, Aki Halme, Tapio Karinsalo, Pekka Iso-Ketola, Matti Mäntysalo and Riku Mäkinen. "Dynamic bending test analysis of inkjet-printed conductors on flexible substrates." In Proceedings of *2012 IEEE 62nd Electronic Components and Technology Conference (ECTC)*, San Diego, CA, USA, May 29 - June 1, pp. 80-85, 2012.

[22] Byoung-Joon Kim, In-Suk Choi and Young-Chang Joo. "Electrical failure and damage analysis of multi-layer metal films on flexible substrate during cyclic bending deformation." In proceedings of 2011 *18th IEEE International Symposium on the Physical and Failure Analysis of Integrated Circuits (IPFA)*, Incheon, South Korea, July 4-7 2011, pp. 1-4, 2011.

[23] Yougen Hu, Tao Zhao, Pengli Zhu, Yu Zhu, Xingtian Shuai, Xianwen Liang, Rong Sun, Daoqiang Daniel Lu and Ching-Ping Wong. "Low cost and highly conductive elastic composites for flexible and printable electronics." *Journal of Materials Chemistry C, Vol.* 4, No. 24, pp. 5839-5848, 2016.

[24] Dadhichi Paretkar, Nicholas J. Glassmaker, Kurt R. Mikeska, Greg Blackman and Anand Jagota. "Adhesion of Screen-Printed Silver Metallization to Crystalline Silicon Solar Cells." *IEEE Journal of Photovoltaics*, Vol. 6, No. 5, pp. 1141-1151, 2016.

[25] K. D. Harris, A. L. Elias and H-J. Chung. "Flexible electronics under strain: a review of mechanical characterization and durability enhancement strategies." *Journal of materials science*, Vol. 51, No. 6, pp. 2771-2805, 2016.

[26] Sara Najafian, Alireza V. Amirkhizi and Scott Stapleton. "Interfacial characterization of flexible hybrid electronics," in Behavior and Mechanics of Multifunctional Materials and Composites XII, Denver, Colorado, Vol. 10596, pp 105961T, 2018.

[27] Hang Chen, Bing-Wei Lu, Yuan Lin and Xue Feng. "Interfacial failure in flexible electronic devices." *IEEE Electron Device Letters*, Vol. 35, No. 1, pp. 132-134, 2014.

[28] Ujjwal Gupta, Jaehyun Park, Hitesh Joshi and Umit Y. Ogras. "Flexibility-aware system-on-polymer (SoP): Concept to prototype." *IEEE Transactions on Multi-Scale Computing Systems*, Vol. 3, No. 1, pp. 36-49, 2017.

[29] Yang Gao, Varun V. Soman, Jack P. Lombardi III, Pravakar P. Rajbhandari, Tara P. Dhakal, Dale Wilson, Mark D. Poliks, Kand Ghose, James N. Turner, Zhangpeng Jin. "Heart Monitor Using Capacitive ECG Electrodes." *Document under preparation.*

[30] Jaehyun Park, Hitesh Joshi, Hyung Gyu Lee, Sayfe Kiaei and Umit Y. Ogras. "Flexible PV-cell Modeling for Energy Harvesting in Wearable IoT Applications." *ACM Transactions on Embedded Computing Systems (TECS)*, Vol. 16, No. 5s, Article 156, 2017.

Varun V. Soman is a Ph.D. candidate in the Department of Systems Science and Industrial Engineering at Binghamton University, Binghamton, New York. He earned his Bachelor's in Mechanical Engineering from University of Pune, Pune, India in 2009 and Master's in Mechanical Engineering from Auburn University, Auburn, Alabama in 2012. His research is in the field of flexible electronics with focus on process development and reliability of flexible hybrid electronics.

Yasser Khan is a postdoctoral scholar in the Department of Chemical Engineering at Stanford University, in Prof. Zhenan Bao's Group. Yasser completed his Ph.D. in Electrical Engineering and Computer Sciences from the University of California, Berkeley, in Prof. Ana Claudia Arias' Group. He received his B.S. in Electrical Engineering from the University of Texas at Dallas, and M.S. in Electrical Engineering from King Abdullah University of Science and Technology. Yasser's research focuses mainly on wearable medical devices, with an emphasis on flexible bioelectronic and biophotonic sensors.

Madina Zabran earned her M.S. in Computer Science from Binghamton University. Her research interests include power efficiency, cyber-physical systems, and medical devices. When Madina isn't programming or researching she likes to take long hikes with her dog.

Dr. Schadt holds Ph.D. (Nanomaterials Chemistry), MS (Organometallic Photochemistry), and MAT (Master of Arts in Teaching Chemistry) graduate degrees. He spent 5-years at *IBM's Thomas J. Watson Research Center in Yorktown Heights, NY* developing photolithographic and vacuum PVD processes supporting the development of multilayer damascene on-chip semiconductor device wiring technologies. He then worked for 9-years in IBM's Microelectronics Division in Endicott, *NY* developing fabrication processes for Polyimide thin-film flexible ball-grid array chip packages; and 3-years at *International Flex Technologies* (IFT) where he was a Senior Engineer responsible for the development, implementation, and manufacturing scale-up of materials and processes used in the Roll-to-Roll fabrication of flexible circuits. Since 2008, Dr. Schadt has been part of the *Materials Research and Development* organization at *i3 Electronics* where he has focused on the fabrication of flexible circuits and rigid circuit boards incorporating liquid crystal polymer (LCP), polyetheretherketone (PEEK), polyphenyl ether (PPE), polyimide (PI) and epoxy dielectric materials for both high-frequency and medical applications. This work has grown to include participation on an NBMC-funded team (*i3 Electronics, Binghamton University* and *UC Berkeley)* that has recently demonstrated the fabrication of a *Flexible Hybrid Electronic* (FHE) *Biometric Human Performance Monitoring* (BHPM) device on a polyimide substrate. He is currently participating in three NextFlex-funded FHE projects that are fostering the development of FHE circuits for sensing applications, and is a member of the both the NBMC and NextFlex Technical Councils. Dr. Schadt holds 9-US patents, has co-authored 27-papers in peer-reviewed journals, and is a contributing author in 2-books.

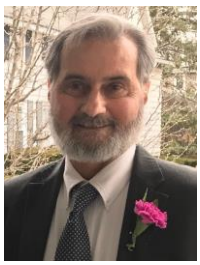

Frank D. Egitto recently retired as Director of Research and Development at i3 Electronics, Inc. in Endicott, NY. Previous work experience included employment with Texas Instruments, Dallas, TX, Applied Materials Plasma Etch Division, Santa Clara, CA, IBM Microelectronics Division, Endicott, NY, and Endicott Interconnect Technologies, Inc., Endicott NY. He holds B.A. and M.A. degrees in physics from Binghamton University and had forty years of experience working in the microelectronics industry.

Konstantinos I. Papathomas, after receiving a B.A. in Chemistry/Mathematics from Saint Anselm College, Manchester NH in 1977 and Ph.D. in Polymer Science/Chemistry from the University of Massachusetts at Lowell, MA, 1981, joined IBM in Endicott, NY as an R/D scientist. He currently holds a senior technologist position with i3 Electronics, Inc. His field of expertise include material synthesis, structure property relationships, material characterization, process development, device encapsulation, adhesives, underfills, formulations design and scale-up, thin film dielectrics, photo-definable permanent dielectrics, environmentally friendly materials, build-up dielectrics and coatings and glass fiber reinforced composites as they pertain to electronic packaging. He is a recipient of over 182 US issued patents and over 50 external technical publications. He has been a member of the American Chemical Society and Polymer Division.

Natasha A. D. Yamamoto is a post-doctoral researcher at University of California, Berkeley, in Prof. Ana C. Arias' Group. She has received her B.S., M.S. and Ph.D. in Physics from Federal University of Parana in Curitiba, Brazil. Her research focuses on wearable devices for health monitoring with an emphasis on solution processed materials and flexible sensors.

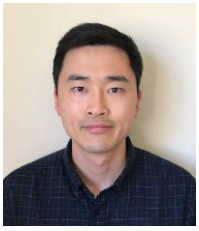

Donggeon Han obtained his Ph.D. in Korea Advanced Institute of Science and Technology (KAIST) in 2015 and now he is a postdoctoral researcher in UC Berkeley. His Ph.D. focus was on reliability of organic photovoltaics (OPVs) and encapsulation, and now he is working on printed organic electronics for various applications.

Ana Claudia Arias is a Professor at the Electrical Engineering and Computer Sciences Department and a faculty director of the Berkeley Wireless Research Center (BWRC) and the Swarm Lab at the University of California in Berkeley. She received her Ph.D. on semiconducting polymer blends for photovoltaic devices from the Physics Department at the University of Cambridge, UK. Prior to that, she received her master and bachelor degrees in Physics from the Federal University of Paraná in Curitiba, Brazil. Her research focuses on devices based on solution processed materials and applications development for flexible sensors and electronic systems.

Kanad Ghose (Ph.D., Iowa State, 1988) is a Professor in the Computer Science Department at the State University of New York at Binghamton, where he served as the Department Chair from 1998 to 2016. His expertise is in power-aware microarchitecture and systems ranging from ultra-low power sensors to high-performance processors and data centers. He has published extensively in these areas and his research work has been funded by NSF, DARPA, AFOSR as well as the industry (Intel, IBM, Lockheed-Martin, BAE Systems, NBMC etc.). Prof. Ghose also serves as the Site Director - Center for Energy-Smart Electronics Systems at Binghamton, a NSF

Industry-University Cooperative Research Center with 6 university sites led by Binghamton. Prof. Ghose has 25 awarded patents, including four licensed patents and is a Fellow of the National Academy of Inventors. He is a member of the IEEE and ACM.

Mark D. Poliks is Empire Innovation Professor of Engineering, Professor of Systems Science and Industrial Engineering and Director of the Center for Advanced Microelectronics Manufacturing (CAMM) at the State University of New York at Binghamton. He holds joint faculty appointment in the Materials Science and Engineering Program and is Chair of the Smart-Energy Transdisciplinary Area of Excellence at Binghamton. His research is in the areas of high performance electronics packaging, flexible hybrid electronics, materials, processing, roll-to-roll manufacturing, in-line quality control and reliability. He is the recipient of the SUNY Chancellor's Award for Excellence in Research. He leads the New York State NextFlex Node and was named a 2017 NextFlex Fellow. He has authored more than one-hundred technical papers and holds forty-six US patents. Previously he held senior technical management positions at IBM Microelectronics and Endicott Interconnect. Poliks is a member of technical councils for the FlexTech Alliance, the Nano-Bio Manufacturing Consortium (NBMC) and NextFlex, and has served on the NextFlex Governing Council. He serves as the General Chair of 69th IEEE/EPS Electronics Components and Technology Conference (ECTC) and recently co-organized a National Science Foundation/NextFlex Workshop on "Accelerating Innovative Manufacturing Technologies for Flexible Hybrid Electronics"

Dr. Turner, Ph.D. is an engineer (B.S.) and biophysicist (Ph.D.) from SUNY at Buffalo with wide ranging experience in the development of instrumentation and technologies for biomedical applications. Much of his work utilizes micro- and nano-fabrication, and the development and application of flexible hybrid electronics. He led the multi-disciplinary/multi-institutional team that developed the human ECG monitor that is the subject of this work.